

# Electrophoretic Motion of Two Spherical Particles with Thick Double Layers

Alexander A. Shugai,\* Steven L. Carnie,\*<sup>1</sup> Derek Y. C. Chan,\* and John L. Anderson†

\*Department of Mathematics, University of Melbourne, Parkville 3052, Australia; and †Department of Chemical Engineering, Carnegie-Mellon University, Pittsburgh, Pennsylvania

Received December 13, 1996; accepted April 8, 1997

The electrophoretic mobilities of two interacting spheres are calculated numerically for arbitrary values of the double-layer thickness. A general formula for the electrophoretic translational and angular velocities of  $N$  interacting particles is derived for low-zeta-potential conditions. The present calculation complements the well-studied case of thin double layers. The results are compared with recent reflection calculations and are used to compute the  $O(\phi)$  contribution to the electrophoretic mobility of a suspension. Particle interactions can be significant for values of the scaled particle radius  $\kappa a \leq 10$ . At  $\kappa a = 1$  the  $O(\phi)$  contribution can increase by a factor of 2–3 over its thin-double-layer value. The precise values depend on the strength of the double-layer repulsions as determined by the particle size. Fluctuations in the electrophoretic velocity are also calculated but would appear to be limited to about 10% of the mean velocity. The reflection results to order  $R^{-6}$ , where  $R$  is the particle separation, are in good agreement with the numerical results for the suspension mobility and fluctuations but higher order reflections produce worse results. Although the effects of pair interactions are noticeable, the major result is that pair interactions even for quite thick double layers are not large. © 1997 Academic Press

**Key Words:** particle interactions; two sphere electrophoresis; electrophoretic mobility; thick double layers.

## 1. INTRODUCTION

Classical electrokinetic theory has been concerned largely with the behavior of dilute suspensions or single particles such as those observed in microelectrophoresis cells (1). In this case, the standard electrokinetic equations need only be solved outside a single particle.

The effect of particle interactions has been well studied in the case of thin double layers, by which we mean  $\kappa a \gg 1$ , where  $a$  is the particle radius and  $\kappa$  is the inverse Debye length of the electrolyte. We assume that our system is in equilibrium with a reservoir of electrolyte which determines  $\kappa$ . The actual determination of the appropriate value of  $\kappa$  to use for a given finite-volume system is not always easy (2).

Two sphere interactions were first explicitly dealt with by reflections for identical spheres (3) and for dissimilar spheres (4). These calculations were checked against exact solutions in bispherical coordinates (5, 6) and boundary collocation techniques, which can be extended to multiparticle interactions (7). These calculations are reviewed in (8).

Similar techniques can be used for the case of polarized thin double layers where  $\kappa a \gg 1$  but

$$\frac{\exp(e|z_i \zeta|/2kT)}{\kappa a} \cong O(1),$$

where  $\zeta$  is the zeta potential of the particle,  $e$  is the protonic charge,  $z_i$  is the valence of ionic species  $i$  in the electrolyte,  $k$  is the Boltzmann constant, and  $T$  is the temperature. Results have appeared for clusters of a few spherical particles (9) and for both ordered and random clusters of up to 64 particles (10).

The chief conclusions of such studies are that particle concentration has a relatively weak effect on electrophoretic mobilities and that identical particles with thin double layers feel no interaction (8). The reason is that, for thin double layers, the charge on the particle is canceled by the charge in the double layer so there is no body force acting on the fluid, unlike the sedimentation problem. The particle moves due to a surface stress caused by the slip velocity boundary condition. The net effect is that particles with separation  $R$  feel interactions decaying as  $R^{-3}$  instead of the long-range  $R^{-1}$  interactions present in sedimentation.

All of this intuition relies on the thin-double-layer approximation, which is appropriate for colloidal suspensions under most conditions but is of less relevance to protein electrophoresis, for example. In this paper, we assess the effect of thick double layers (that is, double-layer thicknesses of the same order as the particle size) on particle interactions by numerical calculations. To keep the calculations feasible, we restrict the analysis to low zeta potentials, which is appropriate for small particles or proteins. Our calculations are thus the two-sphere version of Henry's result for a single sphere (1),

$$\mathbf{U} = \frac{\epsilon_0 \epsilon_r \zeta}{\eta} f(\kappa a) \mathbf{E}_0, \quad [1]$$

<sup>1</sup> To whom correspondence should be addressed.

where  $\mathbf{U}$  is the sphere velocity,  $\mathbf{E}_0$  is the applied electric field,  $\epsilon_0$  is the permittivity of the vacuum,  $\epsilon_r$  is the dielectric constant of the solvent,  $\eta$  is the viscosity, and Henry's function  $f(x)$  is given by

$$f(x) = \frac{2}{3} + \frac{1}{6} x^2 e^x (E_3(x) - E_5(x)) \quad [2]$$

and  $E_n(x)$  is the exponential integral

$$E_n(x) = \int_1^\infty t^{-n} e^{-xt} dt. \quad [3]$$

In the next section we explain the technique we use to calculate the particle mobilities. In Section 3 we present results for the mobilities and compare them with recent reflection calculations on the same system. From the mobilities we obtain the  $O(\phi)$  contribution to the electrophoretic mobility of a suspension in Section 4. Finally we calculate the magnitude of fluctuations in the electrophoretic velocities in Section 5 and finish with discussion.

## 2. METHOD OF CALCULATION

The governing equations describing electrophoresis are by now standard (1). We do not consider embellishments to the simplest model such as Stern layer effects or surface conduction.

We have the following:

1. Poisson's equation describing the electrostatic potential  $\psi$  and charge density  $\rho$  in the solution,

$$\nabla^2 \psi(\mathbf{r}) = - \frac{1}{\epsilon_0 \epsilon_r} \rho(\mathbf{r}),$$

where  $\rho(\mathbf{r}) = \sum z_k e n_k(\mathbf{r})$  and  $n_k(\mathbf{r})$  is the number density of ionic species  $k$ ;

2. the quasistatic inhomogeneous Stokes equations describing the fluid flow,

$$\begin{aligned} \eta \nabla^2 \mathbf{v} - \nabla p &= -\rho \mathbf{E} \\ \nabla \cdot \mathbf{v} &= 0, \end{aligned}$$

where  $p$  is the pressure,  $\mathbf{v}$  is the fluid velocity field, and  $\mathbf{E} = -\nabla \psi$ ;

3. conservation laws for the ion densities,

$$\nabla \cdot (n_i \mathbf{u}_i) = 0,$$

where  $\mathbf{u}_i$  is the velocity of ionic species  $i$ ; and

4. force balance equations on the ionic species,

$$-\lambda_i (\mathbf{u}_i - \mathbf{v}) - z_i e \nabla \psi - kT \nabla \ln(n_i) = \mathbf{0},$$

where  $\lambda_i$  is the drag coefficient of ionic species  $i$ .

With conditions that the electric field tends to the applied field at infinity and the fluid and ionic velocities vanish at infinity, the specification is completed by boundary conditions at the surfaces,

$$\begin{aligned} \psi &= \zeta \\ \text{or} \\ \hat{\mathbf{n}} \cdot \nabla \psi &= - \frac{\sigma}{\epsilon_0 \epsilon_r} \\ \hat{\mathbf{n}} \cdot (\mathbf{u}_i - \mathbf{v}) &= 0 \\ \mathbf{v} &= \mathbf{v}^*, \end{aligned}$$

where  $\sigma$  is the surface charge density of the particle and  $\mathbf{v}^*$  is the velocity of the particle surface, which is  $\mathbf{U} + \boldsymbol{\Omega} \times \mathbf{r}$  for a particle translating with velocity  $\mathbf{U}$  and rotating with angular velocity  $\boldsymbol{\Omega}$ .  $\hat{\mathbf{n}}$  is the unit normal directed into the fluid phase.

In the above equations, we have specified constant potential or constant charge boundary conditions but other, intermediate, boundary conditions could be chosen. For the electrophoresis of a uniform sphere, the electrical surface boundary condition does not affect the electrophoretic velocity (11) but for the two-particle interactions treated here the electrical surface boundary condition does matter, through the equilibrium charge density. We have also set the particle dielectric constant  $\epsilon_p$  to zero; i.e., we have neglected fields internal to the particle, which appears to be reasonable for the common case where  $\epsilon_p \ll \epsilon_r$  (12).

For the case of thin double layers, the above equations simplify in that the charge density is zero outside a thin region surrounding each particle. Instead of solving Poisson's equation and the Stokes equations with body force  $\rho \mathbf{E}$ , one need only solve Laplace's equation and the force-free Stokes equations, albeit with slip velocity boundary conditions. The fact that we must retain the charge density from the diffuse double layer and the body force term precludes techniques such as boundary collocation used in the work cited above (7, 9, 10). We approach the problem in another way—namely the method introduced by Teubner (13), adapted to the two-sphere case.

The main tool of Teubner's approach for hydrodynamic force and torque calculations is a generalized reciprocal theorem. For one particle in an unbounded viscous liquid it is formulated as a relation,

$$\begin{aligned} \eta' \int_S \mathbf{v}' \cdot \boldsymbol{\sigma} \cdot d\mathbf{S} + \eta' \int_G \mathbf{v}' \cdot \mathbf{X} d^3r \\ = \eta \int_S \mathbf{v} \cdot \boldsymbol{\sigma}' \cdot d\mathbf{S} + \eta \int_G \mathbf{v} \cdot \mathbf{X}' d^3r, \end{aligned}$$

connecting the solutions of two systems of Stokes equations for primed and unprimed variables,

$$\begin{aligned}\eta\nabla^2\mathbf{v} &= \nabla p + \mathbf{X}, \quad \nabla \cdot \mathbf{v} = 0, \\ \eta'\nabla'^2\mathbf{v}' &= \nabla p' + \mathbf{X}', \quad \nabla' \cdot \mathbf{v}' = 0.\end{aligned}$$

$G$  is the exterior to a closed surface  $S$ . This reciprocal theorem is valid assuming the quantities  $\mathbf{v}' \cdot \boldsymbol{\sigma}$ ,  $\mathbf{v} \cdot \boldsymbol{\sigma}'$ ,  $\mathbf{v}' \cdot \mathbf{X}$ ,  $\mathbf{v} \cdot \mathbf{X}'$  vanish fast enough far from the particle.

For the same assumptions, the generalization to  $N$  particles is straightforward and gives

$$\begin{aligned}\eta' \sum_{i=1}^N \int_{S_i} \mathbf{v}' \cdot \boldsymbol{\sigma} \cdot d\mathbf{S} + \eta' \int_G \mathbf{v}' \cdot \mathbf{X} d^3r \\ = \eta \sum_{i=1}^N \int_{S_i} \mathbf{v} \cdot \boldsymbol{\sigma}' \cdot d\mathbf{S} + \eta \int_G \mathbf{v} \cdot \mathbf{X}' d^3r, \quad [4]\end{aligned}$$

where now  $G$  is the exterior to all particles,  $G = \mathbf{R}^3 \setminus \cup_{i=1}^N V_i$ .

The force  $\mathbf{F}$  and torque  $\mathbf{T}$  on a particle  $\alpha$  with surface  $S_\alpha$  consist of an electric term and a hydrodynamic term (in what follows, all torques are with respect to the center of the particle). The electric part is

$$\mathbf{F}_\alpha^E = \int_{S_\alpha} \boldsymbol{\sigma}^E \cdot d\mathbf{S}, \quad \mathbf{T}_\alpha^E = \int_{S_\alpha} (\mathbf{r} - \mathbf{r}_\alpha) \times (\boldsymbol{\sigma}^E \cdot d\mathbf{S}), \quad [5]$$

where  $\boldsymbol{\sigma}^E$  is the electrostatic stress tensor and  $\mathbf{r}_\alpha$  is the position of the center of particle  $\alpha$ . Similarly,  $\boldsymbol{\sigma}^H$  is the hydrodynamic stress tensor and the hydrodynamic contribution is

$$\mathbf{F}_\alpha^H = \int_{S_\alpha} \boldsymbol{\sigma}^H \cdot d\mathbf{S}, \quad \mathbf{T}_\alpha^H = \int_{S_\alpha} (\mathbf{r} - \mathbf{r}_\alpha) \times (\boldsymbol{\sigma}^H \cdot d\mathbf{S}). \quad [6]$$

Following Teubner we consider  $6N$  hydrodynamic problems corresponding to unit translations and rotations of each particle in each direction in a liquid with unit viscosity. That is, we define flow fields resulting from particle  $\alpha$  being translated with unit velocity in the  $j$ th direction ( $\bar{\mathbf{V}}_\alpha^j$ ) or being rotated about its center with unit angular velocity about the  $j$ th axis ( $\bar{\mathbf{V}}_\alpha^j$ ), all other particles being fixed. They satisfy the equations

$$\nabla^2 \bar{\mathbf{V}}_\alpha^j = \nabla \bar{p}_\alpha^j, \quad \nabla \cdot \bar{\mathbf{V}}_\alpha^j = 0,$$

$$\bar{\mathbf{V}}_\alpha^j |_{S_l} = \delta_{jk} \delta_{\alpha l}, \quad l = 1, \dots, N, \quad \bar{\mathbf{V}}_\alpha^j \rightarrow 0 \quad \mathbf{r} \rightarrow \infty,$$

$$\nabla^2 \bar{\bar{\mathbf{V}}}_\alpha^j = \nabla \bar{\bar{p}}_\alpha^j, \quad \nabla \cdot \bar{\bar{\mathbf{V}}}_\alpha^j = 0,$$

$$\bar{\bar{\mathbf{V}}}_\alpha^j |_{S_l} = \epsilon_{jmk} (x_m - x_m^\alpha) \delta_{\alpha l}, \quad l = 1, \dots, N,$$

$$\bar{\bar{\mathbf{V}}}_\alpha^j \rightarrow 0 \quad \mathbf{r} \rightarrow \infty.$$

Here  $\alpha = 1, 2, \dots, N$  is a particle index,  $j = 1, 2, 3$  denotes the direction of each translation or rotation, and  $x_m^\alpha$  is the  $m$ th component of  $\mathbf{r}_\alpha$ . These flows have been defined so as to express the hydrodynamic force and torque on particle  $\alpha$  in a form suitable for the reciprocal theorem, Eq. [4]. Now we apply the reciprocal theorem, the primed quantities referring to  $\bar{\mathbf{V}}_\alpha^j$  and  $\bar{\bar{\mathbf{V}}}_\alpha^j$ , and the unprimed ones to  $\mathbf{v}$  at fixed  $\alpha, j$ , to obtain

$$\begin{aligned}F_{\alpha j}^H &= \int_{S_\alpha} \bar{\mathbf{V}}_\alpha^j \cdot \boldsymbol{\sigma} \cdot d\mathbf{S} = \sum_{l=1}^N \int_{S_l} \bar{\mathbf{V}}_\alpha^j \cdot \boldsymbol{\sigma} \cdot d\mathbf{S} \\ &= \eta \sum_{l=1}^N \int_{S_l} \mathbf{v} \cdot \bar{\boldsymbol{\sigma}}_\alpha^j \cdot d\mathbf{S} + \int_G \rho \bar{\mathbf{V}}_\alpha^j \cdot \mathbf{E} d^3r \quad [7]\end{aligned}$$

$$\begin{aligned}T_{\alpha j}^H &= \int_{S_\alpha} \bar{\bar{\mathbf{V}}}_\alpha^j \cdot \boldsymbol{\sigma} \cdot d\mathbf{S} = \sum_{l=1}^N \int_{S_l} \bar{\bar{\mathbf{V}}}_\alpha^j \cdot \boldsymbol{\sigma} \cdot d\mathbf{S} \\ &= \eta \sum_{l=1}^N \int_{S_l} \mathbf{v} \cdot \bar{\bar{\boldsymbol{\sigma}}}_\alpha^j \cdot d\mathbf{S} + \int_G \rho \bar{\bar{\mathbf{V}}}_\alpha^j \cdot \mathbf{E} d^3r. \quad [8]\end{aligned}$$

Here  $\bar{\boldsymbol{\sigma}}_\alpha^j$  and  $\bar{\bar{\boldsymbol{\sigma}}}_\alpha^j$  are the stress tensors for  $\bar{\mathbf{V}}_\alpha^j$  and  $\bar{\bar{\mathbf{V}}}_\alpha^j$ . The sums of the surface integrals on the right-hand side of Eqs. [7] and [8] do not depend on the field  $\mathbf{E}$  since  $\mathbf{v}$  is prescribed on the surface and  $\bar{\boldsymbol{\sigma}}_\alpha^j$  and  $\bar{\bar{\boldsymbol{\sigma}}}_\alpha^j$  are purely hydrodynamic. Thus they represent the force  $\mathbf{F}^{H_0}$  and torque  $\mathbf{T}^{H_0}$  that each particle would experience if it moved at its electrophoretic velocity  $\mathbf{U}$  and angular velocity  $\boldsymbol{\Omega}$  and were neutral. These forces are given in terms of the particle velocities through the grand resistance matrix  $R$  [15]. Therefore we can rewrite the excess hydrodynamic force and torque on the charged particle due to a body force in the Stokes equations as

$$\begin{aligned}F_{\alpha j}^H - F_{\alpha j}^{H_0} &= \int_G \rho \bar{\mathbf{V}}_\alpha^j \cdot \mathbf{E} d^3r \\ T_{\alpha j}^H - T_{\alpha j}^{H_0} &= \int_G \rho \bar{\bar{\mathbf{V}}}_\alpha^j \cdot \mathbf{E} d^3r,\end{aligned}$$

where

$$\begin{pmatrix} \mathbf{F}_1^{H_0} \\ \mathbf{F}_2^{H_0} \\ \vdots \\ \mathbf{F}_N^{H_0} \\ \mathbf{T}_1^{H_0} \\ \mathbf{T}_2^{H_0} \\ \vdots \\ \mathbf{T}_N^{H_0} \end{pmatrix} = -\eta R \begin{pmatrix} \mathbf{U}_1 \\ \mathbf{U}_2 \\ \vdots \\ \mathbf{U}_N \\ \boldsymbol{\Omega}_1 \\ \boldsymbol{\Omega}_2 \\ \vdots \\ \boldsymbol{\Omega}_N \end{pmatrix}.$$

This can be expressed in tensorial notation by defining the hydrodynamic tensors,

$$(\bar{\mathbf{T}}_\alpha)_{kj} = \bar{\mathbf{V}}_{\alpha k}^j$$

$$(\bar{\bar{\mathbf{T}}}_\alpha)_{kj} = \bar{\bar{\mathbf{V}}}_{\alpha k}^j,$$

which are the velocity field generators for the  $\alpha$ th particle moving with translational velocity  $\mathbf{U}$  and rotational velocity  $\mathbf{\Omega}$  when all other particles are at rest:

$$\mathbf{v}(\mathbf{r}) = \mathbf{T}_\alpha(\mathbf{r}) \cdot \mathbf{U} + \bar{\mathbf{T}}_\alpha(\mathbf{r}) \cdot \mathbf{\Omega}.$$

Then the expressions for the excess hydrodynamic force and torque become

$$\mathbf{F}_\alpha^H - \mathbf{F}_\alpha^{H_0} = \int_G \rho \bar{\mathbf{T}}_\alpha^T \cdot \mathbf{E} d^3r \quad [9]$$

$$\mathbf{T}_\alpha^H - \mathbf{T}_\alpha^{H_0} = \int_G \rho \bar{\bar{\mathbf{T}}}_\alpha^T \cdot \mathbf{E} d^3r, \quad [10]$$

where  $\mathbf{A}^T$  denotes the transpose of  $\mathbf{A}$ . This is the analogue of Eq. [23] of Teubner (13).

So far this is still formal because  $\mathbf{E}$  and  $\rho$  depend on the motion. We now make approximations that partially uncouple the flow field from the electric field and reduce the excess hydrodynamic force and torque to known quantities.

First, we consider only weak applied electric fields. This is a standard feature of electrokinetic theory and is a very good approximation for the fields encountered in typical experiments. Next, we consider only a low zeta potential of the particles (the zeta potential  $\zeta$  is taken to be the electrostatic potential at the surface where the hydrodynamic boundary conditions are applied). This is done partly for expedience but also because the thick double layers of interest here often correspond to small particles, typically with quite small zeta potentials. The procedure is then to expand all quantities in a double perturbation series in  $E_0$  and  $\zeta$ , keeping only linear terms.

The result (see (14) for details) is that the governing equations become

$$\left. \begin{aligned} \eta \nabla^2 \mathbf{v}^{(1,1)} - \nabla p^{(1,1)} &= -\rho^{(0,1)} \mathbf{E}^{(1,0)} \\ \nabla \cdot \mathbf{v}^{(1,1)} &= 0, \end{aligned} \right\} \quad [11]$$

where the superscripts denote the order in  $(E_0, \zeta)$  of the quantity. The charge density  $\rho^{(0,1)}$  is the equilibrium charge density calculated from the linearized Poisson–Boltzmann equation

$$\left. \begin{aligned} \nabla^2 \psi &= \kappa^2 \psi \\ \hat{\mathbf{n}} \cdot \nabla \psi|_s &= -\frac{\sigma}{\epsilon_0 \epsilon_r} \text{ or } \psi|_s = \zeta \\ \rho^{(0,1)} &= -\epsilon_0 \epsilon_r \kappa^2 \psi \end{aligned} \right\} \quad [12]$$

and the field  $\mathbf{E}^{(1,0)}$  is the field around neutral particles in the external field  $E_0$

$$\left. \begin{aligned} \nabla^2 \Psi &= 0 \\ \hat{\mathbf{n}} \cdot \nabla \Psi|_s &= 0 \\ \Psi &\rightarrow -\mathbf{E}_0 \cdot \mathbf{r} \text{ as } \mathbf{r} \rightarrow \infty \\ \mathbf{E}^{(1,0)} &= -\nabla \Psi. \end{aligned} \right\} \quad [13]$$

Other electrostatic boundary conditions can be applied—they only affect the conditions for the linearized Poisson–Boltzmann equation.

The key point is, to this order in  $\zeta$ , the ion flux equations and force balance equations do not enter so that the mobilities are independent of ionic drag coefficients. This is equivalent to neglecting the so-called relaxation effect, just as in Henry's original work. In addition, the body force appearing in the Stokes equation is now a known function of position, depending on purely electrostatic quantities.

The problem has been reduced to the following subproblems:

- calculate  $\rho^{(0,1)}$  via the linearized Poisson–Boltzmann equation;
- calculate  $\mathbf{E}^{(1,0)}$  via the Laplace equation;
- calculate the hydrodynamic tensors  $\bar{\mathbf{T}}_\alpha$  and  $\bar{\bar{\mathbf{T}}}_\alpha$ ;
- calculate the hydrodynamic forces and torques  $\mathbf{F}_\alpha^{H_0}$  and  $\mathbf{T}_\alpha^{H_0}$ .

For the case of two spheres, all these problems have been solved.

Since the Stokes equations appear with known body force  $\rho^{(0,1)} \mathbf{E}^{(1,0)}$ , the total force and torque acting on the  $\alpha$ th particle are

$$\begin{aligned} \mathbf{F}_\alpha &= \mathbf{F}_\alpha^H + \mathbf{F}_\alpha^E = \mathbf{F}_\alpha^{H_0} + \int_G \rho^{(0,1)} \bar{\mathbf{T}}_\alpha^T \cdot \mathbf{E}^{(1,0)} d^3r \\ &\quad + \int_{S_\alpha} \sigma^{(0,1)} \mathbf{E}^{(1,0)} dS = \mathbf{F}_\alpha^{H_0} + \mathbf{F}_\alpha^{\text{xs}} \quad [14] \end{aligned}$$

$$\begin{aligned} \mathbf{T}_\alpha &= \mathbf{T}_\alpha^H + \mathbf{T}_\alpha^E = \mathbf{T}_\alpha^{H_0} + \int_G \rho^{(0,1)} \bar{\bar{\mathbf{T}}}_\alpha^T \cdot \mathbf{E}^{(1,0)} d^3r \\ &\quad + \int_{S_\alpha} \sigma^{(0,1)} (\mathbf{r} - \mathbf{r}_\alpha) \times \mathbf{E}^{(1,0)} dS = \mathbf{T}_\alpha^{H_0} + \mathbf{T}_\alpha^{\text{xs}}, \quad [15] \end{aligned}$$

where  $\sigma^{(0,1)}$  is the surface charge density of the particles calculated from the linearized Poisson–Boltzmann equation. This equation is the analogue of Eq. [92] of Teubner, the major difference being that it is no longer possible to convert the electric force and torque on particle  $\alpha$  to a volume integral. The integrals in the expressions for the excess forces and torques  $\mathbf{F}_\alpha^{\text{xs}}$ ,  $\mathbf{T}_\alpha^{\text{xs}}$  do not depend on the actual motion of the particles. If the particles are held fixed in a certain configuration, the hydrodynamic forces and torques vanish but the excess forces and torques survive—one can interpret these as just the (negative of) the forces and torques required

to keep the particles at rest in a given configuration for a given applied electric field.

In the case of the electrophoresis of a group of  $N$  particles the total force and torque on each particle are equal to zero, since we neglect particle inertia,

$$\begin{aligned}\mathbf{F}_\alpha &= \mathbf{F}_\alpha^{\text{H}_0} + \mathbf{F}_\alpha^{\text{xs}} = \mathbf{0} \\ \mathbf{T}_\alpha &= \mathbf{T}_\alpha^{\text{H}_0} + \mathbf{T}_\alpha^{\text{xs}} = \mathbf{0}.\end{aligned}$$

The rest of the calculation follows that in (13). The expressions for  $\mathbf{F}_\alpha^{\text{H}_0}$ ,  $\mathbf{T}_\alpha^{\text{H}_0}$  are known from classical hydrodynamics as linear functions of particle translational and rotational velocities with coefficients which form the grand resistance matrix  $R$  (15, 16).

$$\begin{pmatrix} \mathbf{F}_1^{\text{H}_0} \\ \mathbf{F}_2^{\text{H}_0} \\ \vdots \\ \mathbf{F}_N^{\text{H}_0} \\ \mathbf{T}_1^{\text{H}_0} \\ \mathbf{T}_2^{\text{H}_0} \\ \vdots \\ \mathbf{T}_N^{\text{H}_0} \end{pmatrix} = -\eta R \begin{pmatrix} \mathbf{U}_1 \\ \mathbf{U}_2 \\ \vdots \\ \mathbf{U}_N \\ \boldsymbol{\Omega}_1 \\ \boldsymbol{\Omega}_2 \\ \vdots \\ \boldsymbol{\Omega}_N \end{pmatrix} = - \begin{pmatrix} \mathbf{F}_1^{\text{xs}} \\ \mathbf{F}_2^{\text{xs}} \\ \vdots \\ \mathbf{F}_N^{\text{xs}} \\ \mathbf{T}_1^{\text{xs}} \\ \mathbf{T}_2^{\text{xs}} \\ \vdots \\ \mathbf{T}_N^{\text{xs}} \end{pmatrix} \quad [16]$$

The electrophoretic velocities of the particles can be obtained as a solution of this linear system. Formally, the inverse of the grand resistance matrix forms the grand (electrophoretic) mobility matrix. In principle, these equations provide a framework for the calculation of electrophoretic effects among  $N$  particles. Because the underlying problems, both hydrodynamic and electrostatic, are only known for the case of two spheres, we focus on this case.

### 3. ELECTROPHORETIC MOBILITIES OF TWO SPHERES

We consider two spheres of radii  $a_1$ ,  $a_2$ , zeta potentials  $\zeta_1$ ,  $\zeta_2$ , and center-to-center separation  $R$ .

For the thin-double-layer case, there is no coupling between motion parallel and perpendicular to the line joining the centers of the two spheres. The following argument establishes the same decoupling for the present case of low zeta potential and applied field.

From axial symmetry, it is clear that an electric field in the direction of the line of centers can produce no torque and a force only in the same direction. If the field is perpendicular to the line of centers the excess force from Eq. [14] is in the same direction as the field, using the symmetry of the integrands. Alternatively, reverse the direction of the applied field and use the linearity in  $\mathbf{E}^{(1,0)}$ . In this case, a torque on each particle is generated about an axis perpendicular to both the field and the line of centers. Now using the symmetry of the grand resistance matrix for axisymmetric geometries such as the two-sphere case (16), it follows that

the particle translational and rotational velocities show a similar decoupling; e.g., a field parallel to the line of centers produces translational motion in the direction of the field.

The whole electrophoretic mobility tensor can then be written in terms of three scalars, two translational mobilities and one rotational mobility.

$$\mathbf{U}_\alpha = [\mu_\parallel^\alpha \mathbf{d}\mathbf{d} + \mu_\perp^\alpha (\mathbf{I} - \mathbf{d}\mathbf{d})] \cdot \mathbf{E}_\infty \quad [17]$$

$$\boldsymbol{\Omega}_\alpha = \mu_\Omega^\alpha \mathbf{E}_\infty \times \mathbf{d} \quad [18]$$

These scalars are the equivalent of the quantities  $M^{(n)}$ ,  $M^{(p)}$ , and  $N$  in the thin-double-layer case (9), just with a different choice of normalization. In general, they depend on separation  $R$  and the Debye length  $\kappa^{-1}$ , as well as on the particle radii and zeta potentials.

We have performed calculations for size ratios  $a_1/a_2 = 0.5, 1$ , and  $2$  and potential ratios  $\zeta_1/\zeta_2$  in the range from  $-2$  to  $+2$ . Qualitatively, the results are the same as for the thin-double-layer case (5, 6) in that the small sphere is affected more than the larger particle and, for small separation, may even change its direction of motion. Because our chief interest here is in the suspension mobility, we do not pursue systematic investigation of the case of unequal spheres here but simply observe that the equations described above cater for that case. Similarly, we do not pursue the investigation of the rotational mobility (although we always calculate it in what follows) but concentrate on the translational mobilities of equal-sized spheres.

Because of the linearity with respect to the zeta potential, the solution for any choice of zeta potentials on the two particles can be written as a linear combination of the special cases:

- particles with identical zeta potential,
- particles with equal and opposite zeta potential.

From now on we consider only these special cases.

This leads to the choice of normalization for the translational mobilities,

$$\mathbf{U}_\alpha = \frac{\epsilon_0 \epsilon_r \zeta_\alpha f(\kappa a)}{\eta} [\mu_\parallel \mathbf{d}\mathbf{d} + \mu_\perp (\mathbf{I} - \mathbf{d}\mathbf{d})] \cdot \mathbf{E}_\infty, \quad [19]$$

where  $\mathbf{d}$  is the unit vector in center-center direction,  $\zeta_\alpha$  is the zeta potential of sphere  $\alpha$ , and  $f(\kappa a)$  is the Henry function (see Eqs. [1] and [2]). This equation defines the dimensionless mobilities  $\mu_\parallel$  and  $\mu_\perp$  for the special cases mentioned above, which are functions solely of  $\kappa a$  and  $R/a$ . The pair mobilities will approach the isolated particle mobility  $\mu_0$  at large separations—with this choice of normalization,  $\mu_0$  is just equal to unity.

The electric potential around neutral particles in an external field (the solution to Eq. [13]) is known as an expansion in hyperbolic functions and Legendre polynomials in bi-

spherical coordinates (3, 5, 6). The coefficients in the expansion are obtained as a solution of a banded (six-diagonal) linear system, which can be solved by a banded solver. Once the potential is known, analytic differentiation and conversion from bispherical to Cartesian coordinates produce the electric field vector  $\mathbf{E}^{(1,0)}$ . The number of terms in the expansion is chosen to achieve sufficient accuracy in the integration of the excess force.

The hydrodynamic flow for both perpendicular (17) and parallel (18, 19) cases is known as an expansion in bispherical coordinates as well. The matrix for the perpendicular case now contains 24 diagonals, and Gauss elimination is used to solve the linear system. The coefficients for the Stokes' stream function for the axisymmetric flow of the parallel case are given by explicit formulas. The flow fields are found by analytical differentiation and conversion from bispherical coordinates to Cartesian. The hydrodynamic tensors appearing in the excess force are then just the flow field recovered by choosing particular values for the motion of the spheres; e.g., one sphere moves with unit velocity in the  $x$  direction, the other being held stationary. The elements of the grand resistance matrix can be written as combinations of the flow coefficients for perpendicular and parallel cases and so are easier to obtain than the flow field.

The final piece of information required is the equilibrium charge density as given by the linearized Poisson–Boltzmann equation, Eq. [12].

For separations where there is no significant overlap of the double layers, the superposition approximation would be valid. The volume charge density is then just the sum of the densities for isolated particles. The surface charge density is taken as the charge density of an isolated sphere. Taking results for the double-layer force as a guide, this should be accurate for separations  $\kappa(R - 2a) > 2$  (12), i.e.,  $R/a > 2 + 2/\kappa a$ .

For smaller separations, an accurate solution of the linearized Poisson–Boltzmann equation must be used to calculate the double-layer charge density and surface charge density due to overlapping double layers. The linearized Poisson–Boltzmann equation is not separable in bispherical coordinates so we represent the solution as a multicenter expansion about each sphere. The coefficients can be found by a boundary Galerkin method (20) or boundary collocation (21). The double-layer charge density and surface charge densities can then be calculated for various models of the surface, such as constant potential, constant charge, or an intermediate model termed ‘linear regulation’ by us (22).

For constant charge boundary conditions and the two canonical cases of equal and opposite charged spheres the perpendicular and parallel mobilities are defined now as

$$\mathbf{U} = \frac{\epsilon_0 \epsilon_r \zeta_0(\sigma) f(\kappa a)}{\eta} [\mu_{\parallel} \mathbf{d}\mathbf{d} + \mu_{\perp} (\mathbf{I} - \mathbf{d}\mathbf{d})] \cdot \mathbf{E}_{\infty},$$

where  $\zeta_0(\sigma) = \sigma / (\epsilon_0 \epsilon_r (1 + \kappa a) / a)$  is the potential of an isolated spherical particle with given surface charge density  $\sigma$ .

Linear regulation as a boundary condition which models surface ionization is defined as  $\sigma = S - K\psi$  (22, 23), where the sign of the constant  $S$  is the same as the sign of the surface charge when the particle is in isolation and the constant  $K$  is always positive. For the two canonical cases, the mobilities  $\mu_{\parallel}$ ,  $\mu_{\perp}$  are defined for this model as

$$\mathbf{U} = \frac{\epsilon_0 \epsilon_r \zeta_0(S, K) f(\kappa a)}{\eta} [\mu_{\parallel} \mathbf{d}\mathbf{d} + \mu_{\perp} (\mathbf{I} - \mathbf{d}\mathbf{d})] \cdot \mathbf{E}_{\infty},$$

where  $\zeta_0(S, K) = S / (K + \epsilon_0 \epsilon_r (1 + \kappa a) / a)$  is the zeta potential of an isolated spherical particle with given constants  $S$ ,  $K$ . The constant charge case results from the choice  $K = 0$ . The choice  $K = \epsilon_0 \epsilon_r \kappa$  is a special case ‘‘midway’’ between constant charge and constant potential conditions (22).

Both surface and volume integrals are calculated numerically in bispherical coordinates using product integration with composite closed Newton–Cotes 10-panel formulas. The intervals are subdivided until suitable accuracy is achieved. In all there are 12 integrands, giving the components in Cartesian coordinates of the forces and torques acting on each sphere. The surface integral is invariably of opposite sign to the volume integral so care must be taken to ensure sufficient accuracy in the final result.

The mobilities (translational and rotational velocities for each sphere) are then calculated from the linear system, Eq. [16]. A typical calculation takes from 70 s of CPU time ( $\kappa a = 2$ ) to 300 s ( $\kappa a = 10$ ) on an IBM RISC6000 workstation for  $R/a$  around 3. As  $R/a$  approaches 2, the computational time increases appreciably.

In Figs. 1–4, we show the dimensionless electrophoretic mobilities of each sphere for the case of identical spheres ( $\zeta_1 = \zeta_2$ ) as a function of dimensionless center-to-center separation  $R/a$  for different values of  $\kappa a$ . In this case, the mobilities of each sphere are the same so no relative motion is induced by particle interaction.

Several features are evident at this stage:

1. Unlike the case for thin double layers  $\kappa a \rightarrow \infty$  (8), the results for finite  $\kappa a$  show that the mobility of a pair of identical particles is affected by double-layer interactions. The interaction is fairly weak at large values of  $\kappa a$  (see Figs. 3 and 4 for  $\kappa a = 10, 30$  and note the scale change) but becomes more significant at low values of  $\kappa a$ .

2. The deviation of the mobilities for different models of the surface (constant potential, constant charge or linear regulation), as well as the superposition approximation, begins with the overlapping of the double layers when the surface-to-surface separation between spheres is about 5 Debye lengths. At these separations and closer, the behavior

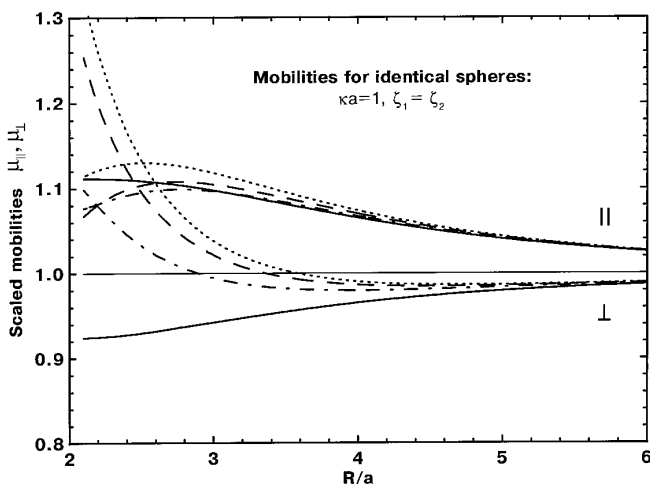


**FIG. 1.** The dimensionless electrophoretic mobilities of each sphere for the case of identical spheres ( $a_1 = a_2$ ,  $\zeta_1 = \zeta_2$ ). The top set of curves refers to  $\mu_{||}$ ; the bottom set refers to  $\mu_{\perp}$ . The horizontal line is the result for an isolated sphere. The different curves are for the case of constant potential boundary conditions (solid line), linear regulation (dot-dashed line) with  $K = \epsilon_0 \epsilon_r \kappa$ , constant charge (dashed line), and the superposition approximation (dotted line). The value of  $\kappa a$  is 1.

of the mobility curves depends on the type of boundary condition. The mobilities for the superposition approximation are shown for illustrative purposes only because the nonelectroneutrality of this approximation makes them not physical at small separations. For larger separations it is evident that use of the superposition approximation is justifiable.

3. In every case, the mobilities corresponding to the linear regulation model lie between those for constant potential and those for constant charge boundary conditions, which is comforting.

The marked deviations of the constant charge result from

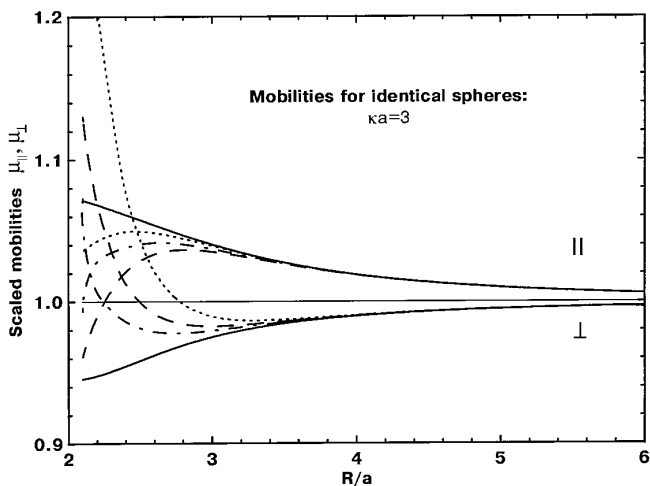


**FIG. 2.** As for Fig. 1, but for  $\kappa a = 3$ .

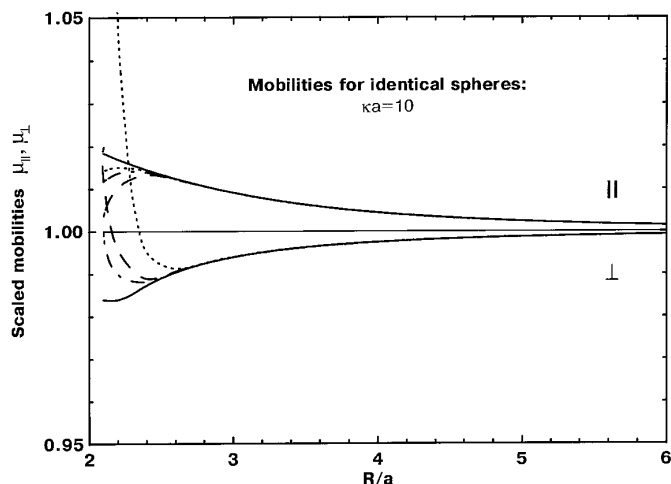


**FIG. 3.** As for Fig. 1, but for  $\kappa a = 10$ .

the constant potential results at small separations and low  $\kappa a$  are due to the growth in the surface potentials as the particles approach each other at constant charge. The potentials then become so large that the assumption of low zeta potential becomes questionable.

Corresponding results for oppositely charged but equal-sized opposite spheres are shown in Figs. 5–7. The effect is much stronger for unlike particles—for  $\kappa a = 10$  the mobilities can change by 20% at  $R/a = 2.5$  compared to 1 or 2% for identical particles. In the constant charge case, the surface potentials actually fall as the spheres approach so the assumption of low zeta potential becomes more realistic. The deviation of the curves for different models of the surface in the case of oppositely charged particles is significantly smaller than that for identical spheres. The explanation is that due to the antisymmetry about the midplane, all surface models, as well as the superposition approximation, have the same charge density at the midplane, viz.  $\rho^{(0,1)}$

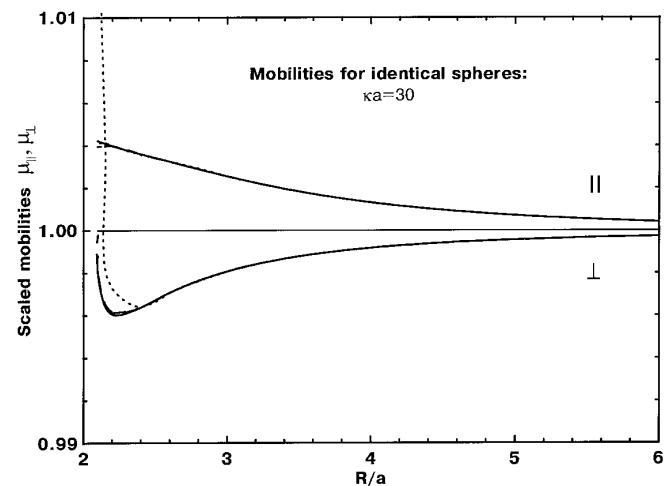


**FIG. 4.** As for Fig. 1, but for  $\kappa a = 30$ .

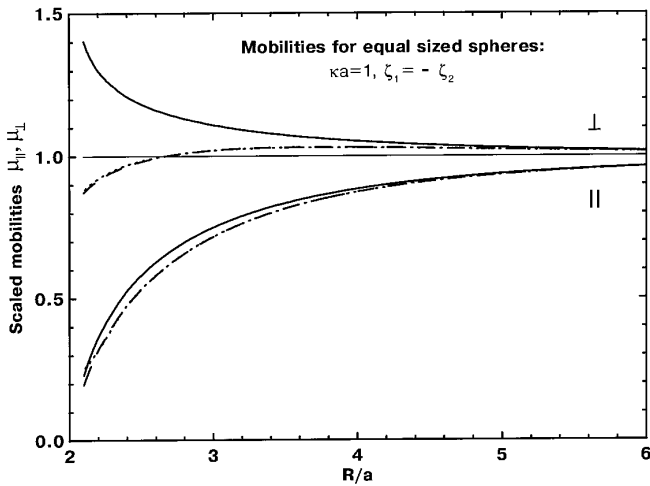


FIG. 5. As for Fig. 1, but for oppositely charged particles ( $\zeta_1 = -\zeta_2$ ). No linear regulation results are shown.

$= 0$ . This suggests that the differences in charge density distributions for different surface models are smaller for oppositely charged spheres than for identical spheres. This is reflected in the mobility curves since the charge density is in effect a weighting factor in the integrals that determine the particle forces and torques.

The general pattern of the deviations from the single particle mobility can be explained in terms of the action of the leading order  $1/r^3$  flow and electric fields, set up by each sphere, acting on the other sphere. Due to the dipolar nature of these fields, the deviation for pairs aligned parallel to the field are twice as large and opposite in sign to those for perpendicular alignment. The net effect depends on the balance between electric and flow fields, but electric field effects appear to be less important, except possibly at low separations.

For identical particles aligned parallel to the field, the flow

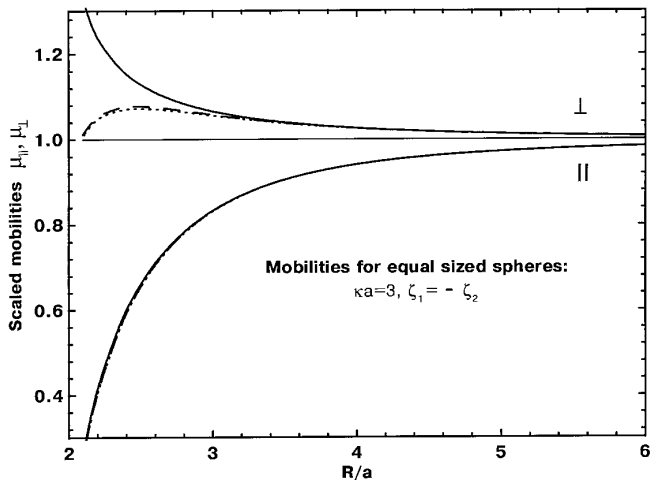


FIG. 6. As for Fig. 5, but for  $\kappa a = 3$ .

field set up by each particle speeds up the other particle so that  $\mu_{\parallel} \geq \mu_0$ . When aligned perpendicular to the flow, the flow fields retard the other sphere so  $\mu_{\perp} \leq \mu_0$ .

Oppositely charged particles move in opposite directions so the flow fields act in the opposite sense—the above inequalities are then reversed. Similar results for this case are seen with thin double layers (3).

Some explanation of the relative behavior of the various mobility curves can be given for the parallel case. For the perpendicular case, the situation is complicated by coupling between translation and rotation so that mobilities are determined as a solution of a linear system involving the calculated forces and torques.

For the parallel case, larger forces mean larger mobilities since there is no translation–rotation coupling. The various mobility curves differ only because of the charge densities  $\rho^{(0,1)}$  and  $\sigma^{(0,1)}$ , which act as weighting factors inside the volume and surface integrals, respectively. From inspection of the calculated values of the charge densities and from the known behavior of the linearized Poisson–Boltzmann equation charge density, we obtain the following inequalities for identical spheres:

$$|\rho_{cc}| > |\rho_{sup}| > |\rho_{cp}|, |\sigma_{cc}| = |\sigma_{sup}| > |\sigma_{cp}|.$$

Here the subscripts cc, cp, and sup refer to constant charge, constant potential boundary conditions, and the superposition approximation, respectively. From this we get the following inequalities for the corresponding volume and surface integrals:

$$|V_{cc}| > |V_{sup}| > |V_{cp}|, |S_{cc}| = |S_{sup}| > |S_{cp}|.$$

The volume integrals always have the opposite sign to the surface integrals. Unfortunately the inequalities cannot be

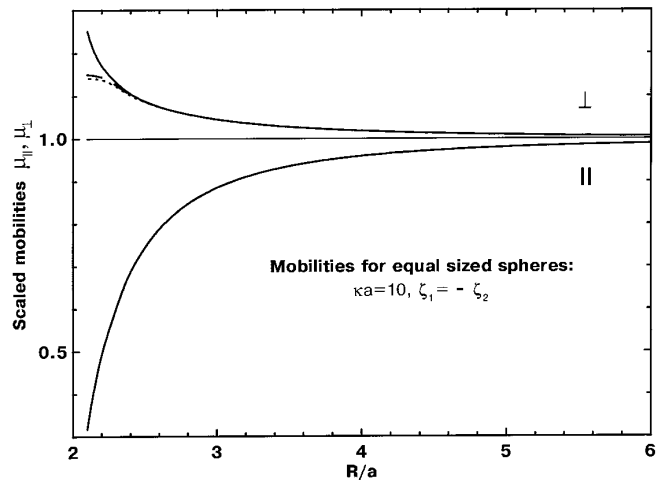


FIG. 7. As for Fig. 5, but for  $\kappa a = 10$ .

subtracted, so the only consequence is  $|S_{cc}| - |V_{cc}| < |S_{sup}| - |V_{sup}|$ , which means  $F_{cc} < F_{sup} \Rightarrow \mu_{||cc} < \mu_{||sup}$  for identical spheres in accordance with the numerical results.

For small  $\kappa a$ , the volume integral becomes dominated by the surface integral. Under these conditions, the inequalities above yield  $|S_{cc}| > |S_{cp}| \Rightarrow F_{cc} > F_{cp} \Rightarrow \mu_{||cc} > \mu_{||cp}$  as seen at  $\kappa a = 1$  in Fig. 1. This reversal of the usual ordering with respect to surface boundary conditions first occurs at  $\kappa a = 2$  and becomes more pronounced as  $\kappa a$  decreases.

In our initial investigations, we tried evaluating the excess force integrals using far-field expressions to  $O(1/R^5)$  for the hydrodynamic tensors, electric field, and resistance matrix (24), together with the superposition approximation. Although the results are quite comparable to those shown for nonoverlapping double layers for oppositely charged spheres, they are unacceptably inaccurate for identical spheres. We interpret this as a fixed absolute error becoming more noticeable in calculating the small deviations found for identical particles.

Recently, reflection calculations have been performed for the same conditions as studied here (25). These produce asymptotic expressions for the particle mobilities as expansions in  $a/R$ . The nature of the electrostatic boundary condition at the surface never enters the reflection calculations, so they are limited to cases where  $\kappa(R - 2a) > 5$ . For this reason, we do not compare the two sets of results at  $\kappa a = 1$  because the interaction there is dominated by the overlapping double layers. Subject to this restriction, it is desirable to gauge the region of validity of the reflection calculations because, as analytical formulas, they are much easier to use than the numerical approach outlined here.

We compare the two approaches in Fig. 8 for identical spheres and in Fig. 9 for oppositely charged spheres. The

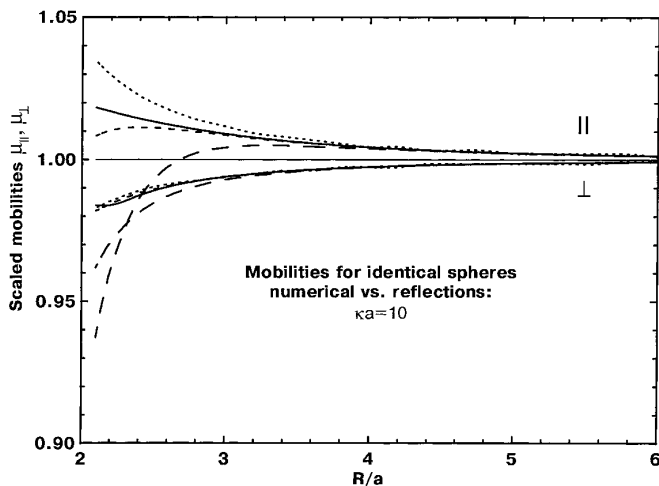


FIG. 8. Electrophoretic mobilities for identical spheres at  $\kappa a = 10$  calculated numerically (constant potential boundary conditions) compared to the results of reflection calculations (25). Solid curves are the numerical results. Reflection calculations shown are accurate to  $O(1/R^3)$  (dotted line),  $O(1/R^6)$  (short dashed line), and  $O(1/R^9)$  (dashed line).

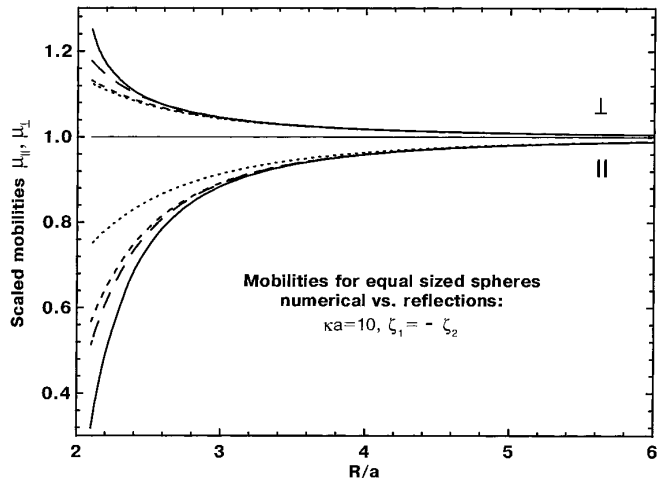


FIG. 9. As for Fig. 8, but for oppositely charged particles ( $\zeta_1 = -\zeta_2$ ).

results shown are for  $\kappa a = 10$  but results for  $\kappa a = 3-30$  all show similar behavior.

For identical spheres, the reflection results are given for the cases where all terms of order  $R^{-3}$ ,  $R^{-6}$ , and  $R^{-9}$  are included. There are significant differences among these expansions for  $R/a < 3$ . For  $R/a > 4$ , the three expansions agree with each other and with the numerical value. For oppositely charged spheres, the reflection results appear to be better behaved and give acceptable results for  $R/a > 3$ . These regions are only achievable for nonoverlapping double layers if  $\kappa a > 3-5$ . From these figures one would choose the reflection results to order  $R^{-6}$  as the analytical expression closest to the numerical results.

The issue of how well the reflection results agree with the numerical values also arises in the next section, where we use the pair mobilities to calculate the suspension mobility to first order in the volume fraction  $\phi$ .

#### 4. $O(\phi)$ —CORRECTION TO THE MOBILITY OF A DILUTE SUSPENSION

Probably the chief purpose of calculating the pair mobilities in the previous section is to assess the volume-fraction dependence of the measured mobility of a random suspension. The derivation of expressions for the suspension electrophoretic mobility is not trivial, involving renormalization techniques similar to those originally used for the sedimentation problem (26, 27). To the first order in the volume fraction of particles  $\phi$  and to  $O(\zeta)$ , the suspension mobility  $\mu_{susp}$  has recently been derived for the case of a mildly polydisperse suspension (25). The main assumptions in the derivation are that the Peclet number for relative motion of the particles is small and that the direct contribution of Brownian motion is negligible (the role of Brownian motion is to maintain the isotropic nature of the pair correlations in the suspension). For the case of a precisely monodisperse sus-

pension both these assumptions are satisfied and the suspension mobility, in terms of the isolated particle mobility  $\mu_0$ , is given by

$$\frac{\mu_{\text{susp}}}{\mu_0} = 1 + \phi \left\{ -\frac{3}{2} + \frac{K(\kappa a)}{f(\kappa a)} + \int_2^\infty g(u) u^2 [\mu_{\parallel} + 2\mu_{\perp} - 3] du \right\} + O(\phi^2), \quad [20]$$

where  $u = R/a$ ,  $g(u)$  is the pair correlation function for the particles and

$$K(\kappa a) = -\frac{2}{\kappa a} - \frac{2}{(\kappa a)^2} - \frac{\kappa a}{15} - \frac{(\kappa a)^2}{30} e^{\kappa a} (3E_5(\kappa a) - 5E_3(\kappa a)).$$

It should be mentioned that the term  $-3/2$  derived in (27) does not agree with experiments on ghost red blood cells (28) which show a term of  $-1$ . The term involving  $K(\kappa a)$  arises from the renormalization of the expression for the suspension mobility using the constraint of zero volume-averaged velocity. It vanishes as the double layer becomes thin ( $\kappa a \rightarrow \infty$ ).

To lowest order in volume fraction, the pair correlation function is given by

$$g(u) = \exp[-\Phi(R/a)/kT], \quad [21]$$

where  $\Phi(u)$  is the interaction potential between particles. The simplest such choice, which amounts to neglecting the double-layer forces between the particles, is a hard-sphere potential for which

$$g^{\text{HS}}(u) = \begin{cases} 0 & \text{for } u < 2 \\ 1 & \text{for } u \geq 2. \end{cases} \quad [22]$$

This is the choice used for thin double layers because of the separation of length scales between the double-layer interactions and the hydrodynamic interactions (7).

Using this choice for  $g^{\text{HS}}(u)$ , the suspension mobility can then be calculated as

$$\frac{\mu_{\text{susp}}}{\mu_0} = 1 + \phi \left( -\frac{3}{2} + \frac{K(\kappa a)}{f(\kappa a)} + \int_2^\infty u^2 [\mu_{\parallel} + 2\mu_{\perp} - 3] du \right) + O(\phi^2). \quad [23]$$

For thin double layers ( $\kappa a \rightarrow \infty$ ), only the first term survives

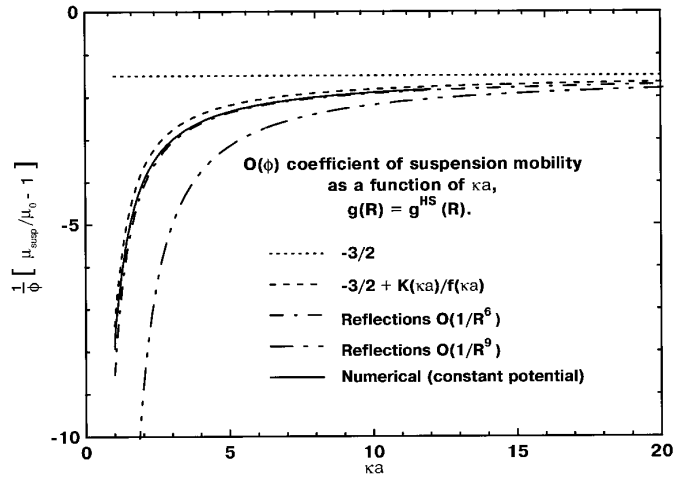


**FIG. 10.** The  $O(\phi)$  coefficient of suspension mobility as a function of  $\kappa a$  for  $g(R) = g^{\text{HS}}(R)$  (Eq. [22]). Numerical results for constant potential (solid line), the thin-double-layer limit ( $-3/2$ ), and the contribution from the second term in Eq. [23] are shown. Also shown are reflection results to  $O(R^{-6})$  and  $O(R^{-9})$ .

since  $K(\kappa a)$  vanishes in this limit and the pair mobilities equal the isolated sphere values so the integrand vanishes. The major interest, then, is the magnitude of the other terms in the  $O(\phi)$  coefficient compared to the ever-present  $-3/2$ .

The integral over  $[2, \infty)$  was split into a tail defined on the interval  $[6, \infty)$ , which was calculated analytically using the reflection expressions, and an integral over the interval  $[2, 6]$ , which was done numerically using adaptive open formulas and checked with a Gaussian 10-knot formula. The relative error is below 0.3%. Open formulas are necessary because it is not possible to evaluate the pair mobilities at contact ( $u = 2$ ). The computational effort required is determined by the evaluation of the mobilities at close separations: the closest separation in the adaptive method is  $\approx 2.1$  and in the Gaussian formula,  $\approx 2.05$ . We are limited to such separations because we have used the expansion in bispherical coordinates for the hydrodynamic subproblem. To reach smaller separations we would need to use, for example, boundary collocation techniques to solve the hydrodynamics.

In Fig. 10 we show the contributions to the suspension mobility as a function of  $\kappa a$  using a hard-sphere correlation function. The contribution from the second term in Eq. [23] becomes significant for  $\kappa a \leq 10$ , whereas the integral over pair mobilities gives a fairly small contribution for the constant potential conditions shown here. The reflection results to order  $R^{-6}$  are rather close to the numerical result, which is consistent with the general accuracy for the pair mobilities themselves for  $\kappa a \geq 10$  (see Figs. 8 and 9). For smaller values of  $\kappa a$ , where the important contributions from the pair mobilities correspond to substantial double-layer overlap, the close agreement must be regarded as fortuitous.

The sensitivity of the result to surface boundary condition is seen in Fig. 11, which shows the  $O(\phi)$  coefficient of suspension mobility as a function of  $\kappa a$  for constant charge, constant potential, and linear regulation ( $K = \epsilon_0 \epsilon_r \kappa$ ) boundary conditions.

The calculations resulting in Figs. 10 and 11 are rather time consuming, since they require values of the pair mobilities at close separations. For the values of  $\kappa a$  where the results depend on the surface boundary condition, the regions of double-layer overlap contribute significantly to the pair mobilities. This suggests we should include the effect of double-layer overlap on the pair distribution functions.

In calculating the excess force in Eq. [14], we have included an excess force of order  $O(\zeta E_0)$  but neglected the double-layer force of order  $O(\zeta^2 e^{-\kappa h})$ . Once the double layers overlap significantly this is of order  $O(\zeta^2)$ . Now the applied electric field is generally much weaker than the field in the double layer, i.e.,  $E_0 \ll \zeta \kappa$ , which suggests that the double-layer forces, for significant overlap, are more important than the forces we have included to generate the pair mobilities.

It is not hard to see that it is permissible to neglect the double-layer forces in Eq. [14] (they produce no torque) because they act along the line of centers between pairs of particles and so give no contribution to the net electrophoretic drift in the direction of  $\mathbf{E}_0$ . However, the argument above shows that we must include double-layer forces through the choice of pair distribution function.

We have chosen an approximate analytic form for the double-layer force for low surface potentials that has been tested against numerical results at constant potential (29, 30):

$$g^{\text{dl}}(R) = \exp[-\Phi_{\text{dl}}(R)/kT]$$

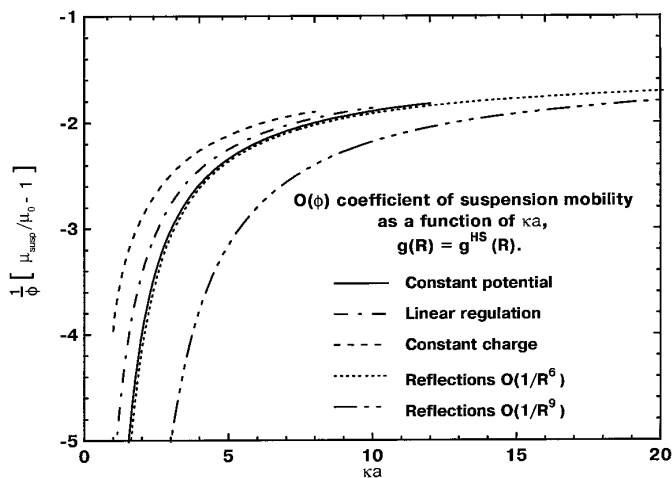


**FIG. 11.** The  $O(\phi)$  coefficient of suspension mobility as a function of  $\kappa a$  for  $g(R) = g^{\text{HS}}(R)$ . The different curves are for the case of constant potential boundary conditions (solid line), linear regulation (dot-dashed line) with  $K = \epsilon_0 \epsilon_r \kappa$ , and constant charge (dashed line).

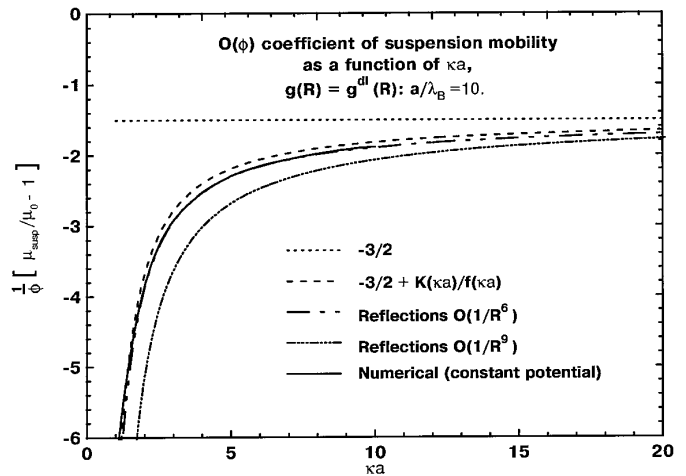


**FIG. 12.** As for Fig. 10 but with  $g(R)$  given by Eq. [25] for  $a/\lambda_B = 10$ .

$$\frac{\Phi_{\text{dl}}}{a\epsilon\zeta^2} = \frac{a}{R} \log(1 + e^{-\kappa h}).$$

In dimensionless form, the pair-correlation function is

$$g^{\text{dl}}(u) = \exp[-U_{\text{dl}}(u)], \quad [24]$$

$$U_{\text{dl}}(u) = \bar{\varphi}^2 \frac{a}{\lambda_B} \frac{1}{u} \log(1 + e^{-\kappa a(u-2)}), \quad [25]$$

where  $\bar{\varphi} = e\zeta/kT$  and  $\lambda_B = e^2/4\pi\epsilon_0\epsilon_r kT$  is the Bjerrum length, about 7 Å for water at room temperature.

It follows from Eq. [25] that the particle size no longer enters solely through  $\kappa a$  but also through the ratio  $a/\lambda_B$ , which determines how fast the pair-correlation function changes from 0 to 1. It measures the “strength” of the double-layer forces for fixed  $\zeta$ . We choose two values covering most cases:  $a/\lambda_B = 10$  (typical for proteins) and  $a/\lambda_B = 1000$  (colloidal particles). By assumption the suspension is a stable one so we may neglect attractive forces—we have checked this using typical water/hydrocarbon/water Hamaker constants and find that the lowest value of  $a/\lambda_B = 10$  produces suspensions that are only just stable so lower values are not realistic. Nevertheless these two values should cover most possible behaviors.

In Figs. 12 and 13 we show the various contributions to the suspension mobility as in Fig. 10 but with double-layer forces included in the pair-distribution function. The case of weak repulsions ( $a/\lambda_B = 10$ ) is in Fig. 12 and strong repulsions ( $a/\lambda_B = 1000$ ) in Fig. 13. Once double-layer repulsions are included, the particles rarely sample the small-separation region where the pair mobilities differ most markedly from the single-particle value. The  $O(\phi)$  coefficient is reduced by the double-layer repulsion, the reduction becoming more marked as the “strength” of the double-layer re-

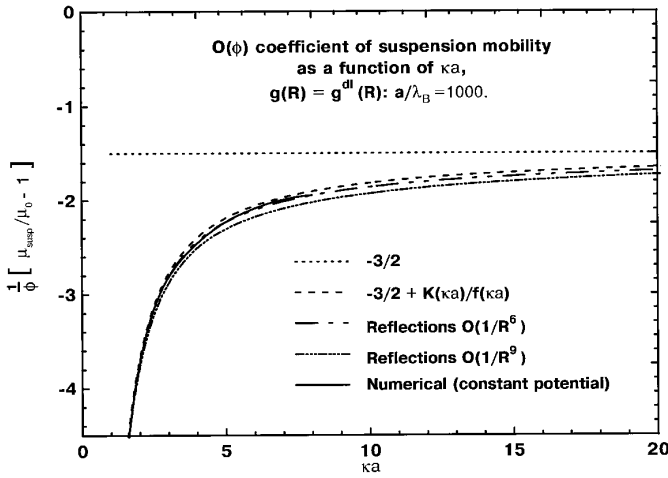


FIG. 13. As for Fig. 12 but for  $a/\lambda_B = 1000$ .

pulsion (the size of the particles) increases. In Fig. 12 the integral over the pair mobilities is still significant. In Fig. 13, by contrast, the contribution of the pair mobilities is so small that for  $\kappa a \geq 2$  the  $O(\phi)$  coefficient is well approximated by just the first two terms, which are analytic! As before, the reflection results to order  $R^{-6}$  are close to the numerical result. From these results, there seems to be no reason to use the reflection results to order  $R^{-9}$ —there is never a case when they are more accurate than the simpler results to order  $R^{-6}$ . Since the particles rarely sample the overlap region, one would expect the results to be insensitive to the surface boundary condition. Examination of the results for constant charge and constant potential boundary conditions show this to be born out.

Since the double-layer forces should always be included in the weighting of the pair mobility contribution, the sensitivity to surface boundary condition seen in Fig. 11 is in fact unrealistic. In practice, it appears to be adequate to use reflection results to order  $R^{-6}$ , weighted by the appropriate pair distribution function, or even the analytic expression given by the first two terms of the  $O(\phi)$  expression in Eq. [20].

## 5. FIELD-INDUCED VELOCITY FLUCTUATIONS

In (25) expressions for the mean square fluctuations in electrophoretic velocity of a monodisperse suspension are derived to  $O(\phi)$ . Expressions are also given for the mean square deviations in the direction of the field—the ratio of these expressions gives the anisotropy of the fluctuations. These velocity fluctuations arise from the random positions of pairs in the suspension rather than from Brownian effects, which give an extra isotropic contribution. The other defining characteristic of these fluctuations is that they depend on the applied field (as  $E_0^2$ ), hence the term field-induced fluctuations.

The fluctuations are given by

$$\langle |\mathbf{U} - \mathbf{U}^{(0)}|^2 \rangle = (U^{(0)})^2 \phi \int_2^\infty g(u) u^2 \times [\mu_{\parallel}(\mu_{\parallel} - 2) + 2\mu_{\perp}(\mu_{\perp} - 2) + 3] du \quad [26]$$

$$\langle |\mathbf{U}_{\parallel} - \mathbf{U}^{(0)}|^2 \rangle = (U^{(0)})^2 \phi \int_2^\infty g(u) u^2 \times \left[ \frac{3}{5} \mu_{\parallel}^2 + \frac{4}{5} \mu_{\parallel} \mu_{\perp} - 2\mu_{\parallel} + \frac{8}{5} \mu_{\perp}^2 - 4\mu_{\perp} + 3 \right] du, \quad [27]$$

where  $\mathbf{U}^{(0)}$  is the isolated particle velocity.

It was found in (25) that the fluctuations could become substantial for  $\kappa a \leq 10$  but this was based on reflection results for the pair mobilities and use of the hard-sphere  $g(R)$ . Since the pair mobilities from the method of reflection results are inaccurate at close separations for these values of  $\kappa a$  it is necessary to assess the significance of velocity fluctuations from a numerical calculation.

In Fig. 14 we show the mean square velocity fluctuations as a function of  $\kappa a$  using the hard-sphere  $g(R)$ . Results for constant charge and constant potential are shown, along with reflection results of various orders. They show that there is no improvement in the reflection results with increasing order—in fact, the  $O(R^{-9})$  results are significantly worse than either the  $O(R^{-3})$  or the  $O(R^{-6})$  results. Analytical expressions for the  $O(R^{-6})$  case are given in (25).

Following the same argument as in the previous section, we should really include double-layer forces in the pair correlation function  $g(R)$  in Eq. [27]. Again, we consider two cases: weak double-layer forces ( $a/\lambda_B = 10$ ) and strong

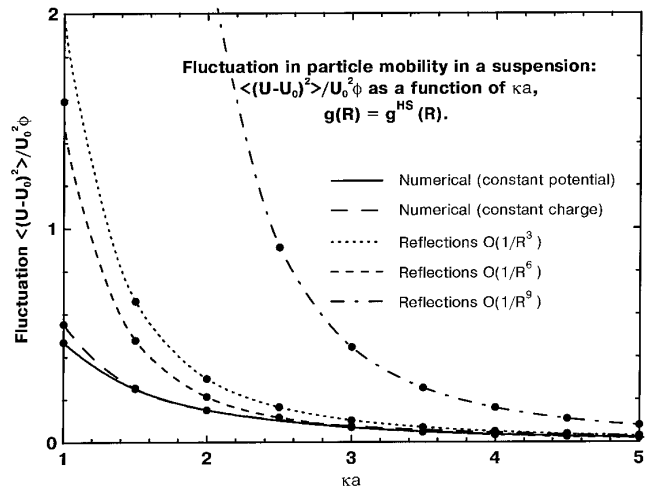


FIG. 14. Mean square velocity fluctuations as a function of  $\kappa a$  for  $g(R) = g^{\text{HS}}(R)$ . The different curves are for the case of constant potential boundary conditions (solid line), constant charge (dashed line), and reflection results of various orders.

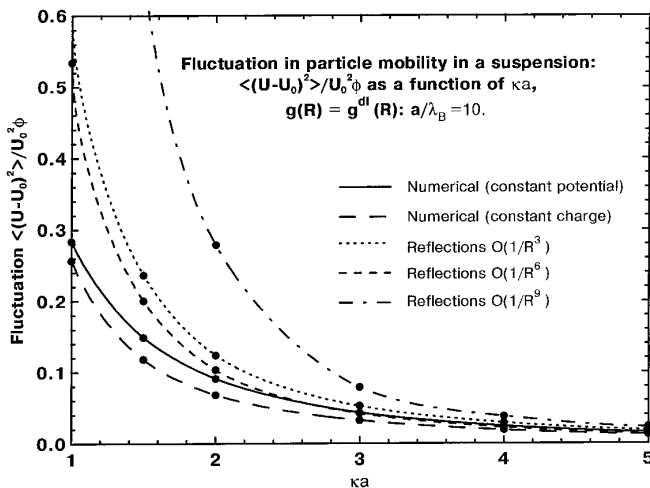


FIG. 15. As for Fig. 14 but with  $g(R)$  given by Eq. [25] for  $a/\lambda_B = 10$ .

forces ( $a/\lambda_B = 1000$ ). In Fig. 15 we show the fluctuations for the case  $a/\lambda_B = 10$ —the chief feature being the change of scale. Just as for the  $O(\phi)$  coefficient, the presence of double-layer forces weakens the effect of the pair mobilities at small separations and so reduces the magnitude of the fluctuations. For strong double-layer repulsion  $a/\lambda_B = 1000$  the effect is even more dramatic (Fig. 16)—the magnitude of the fluctuations is very small and the results are independent of the boundary condition and the number of terms retained in the reflection expansions.

Very similar curves could be plotted for the fluctuations parallel to the field. Instead we give the ratio

$$\frac{\langle |U_{\parallel} - U^{(0)}|^2 \rangle}{\langle |U - U^{(0)}|^2 \rangle},$$

which would be 1/3 for isotropic fluctuations and increases toward 1 for fluctuations preferentially in the direction of the field. The results are virtually constant for  $\kappa a$  in the range 1–5 so we give the figures at  $\kappa a = 1$  in Table 1. The only exception to this is the constant charge case which falls to a ratio of 0.57 (hard sphere) and 0.43 (weak repulsion) as  $\kappa a$  reaches 5.

From these figures we see that as electrostatic repulsion is included or  $\kappa a$  increases, the anisotropy in the constant charge case weakens. The predictions from reflection results to order  $R^{-6}$  agree quite well with the numerical values, but there is no sign, at least for  $\kappa a \leq 5$ , of the large anisotropies predicted from the  $O(R^{-9})$  reflections in (25). In summary, the fluctuations appear in most circumstances to be only moderately anisotropic.

## 6. DISCUSSION

The object of this investigation was to assess how far the insight into particle interactions in electrokinetics obtained

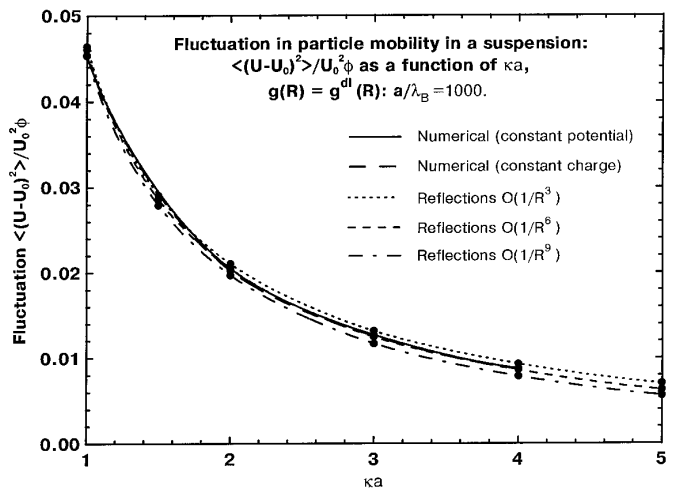


FIG. 16. As for Fig. 15 but for  $a/\lambda_B = 1000$ .

from studies on thin double-layer systems could be taken over into systems with  $\kappa a = O(1)$ . In order to make progress, it is necessary to consider low zeta potentials, both for analytical work (14, 25) and in the present work. The analytical results in (25) showed that to leading order the interaction has the same distance dependence ( $R^{-3}$ ) but that the coefficient depends on  $\kappa a$  and can become large. Our numerical results quantitatively confirm the reflection results for  $R/a \geq 4$  if there is no double-layer overlap and show the effect of particle interactions on pair mobilities for smaller separations, where reflections are in principle unreliable, and for the case of double-layer overlap, where reflections cannot handle by construction. The general conclusion is that the particle velocities are only marginally affected for  $\kappa a \geq 10$ .

As far as suspension properties are concerned, the choice of a pair-correlation function has some effect on the mean mobility and a large influence on the fluctuations about the mean. This choice never enters in the thin-double-layer case since electrostatic repulsions occur over such a small scale compared to the hydrodynamic interactions.

If double-layer repulsions are neglected, the  $O(\phi)$  coefficient of suspension mobility is predicted to change significantly from its thin-double-layer value as  $\kappa a$  approaches 1.

TABLE 1  
The Ratio  $\langle(U_{\parallel} - U^{(0)})^2\rangle/\langle(U - U^{(0)})^2\rangle$  for Numerical and Reflection Results at  $\kappa a = 1$

	$g(R)$		
	Hard sphere	Weak repulsion $a/\lambda_B = 10$	Strong repulsion $a/\lambda_B = 1000$
Constant potential	0.40	0.40	0.40
Constant charge	0.69	0.50	0.40
Reflections $O(R^{-3})$	0.40	0.40	0.40
Reflections $O(R^{-6})$	0.42	0.41	0.40

Similarly, fluctuations can be relatively large. As double-layer effects are included, however, the predicted magnitude of the fluctuations decrease as the size of the particle increases (for a given  $\kappa a$ ). At  $\kappa a = 1-2$  the  $O(\phi)$  coefficient can still be 2–3 times its thin-double-layer value (depending on the particle size) so the effect is still significant.

To estimate the absolute size of these effects, we need to guess to what values of volume fraction they apply. In general this is hard to estimate in the absence of data or terms of  $O(\phi^2)$  but suppose the results are valid up to  $\phi = 0.1$ . Then the suspension mobility at that volume fraction would be expected to decrease from 85% of the dilute value to 70% of the dilute value at  $\kappa a = 2$  for strong repulsions or slightly less for weaker repulsions. The velocity fluctuations at  $\kappa a = 1$  would amount to 7% of the mean velocity for strong repulsions up to 16% of the mean velocity for weak repulsions. For a more typical volume fraction of  $\phi = 0.01$ , these numbers become 2 and 5%, respectively. All of the interaction effects are negligible for  $\kappa a$  much above 10.

Fluctuations in mobility of this size should be compared with other possible sources of variation in mobility. We mention two here—the effect of a distribution in particle size on the single particle mobility and the effect of nonuniform potential of a spherical particle. Another potential source, which we do not discuss here, is the fluctuations due to the varying orientations of a nonspherical particle in the electric field.

Assuming no variation in the zeta potential, a distribution of particle size will produce a distribution of particle velocity through the function  $f(\kappa a)$  in Eq. [2]. A simple calculation shows that the relative rms fluctuations in velocity are related to the standard error in particle size through the function

$$\frac{\kappa a f'(\kappa a)}{f(\kappa a)},$$

which has a maximum value of 0.11 at  $\kappa a$  around 7. This means that at least a 9% variation in particle size is required to produce a 1% variation in mobility at  $\kappa a = 7$  and much more for most other values. Of course, since the mobility is linear in the zeta potential, a 1% variation in  $\zeta$  produces a 1% variation in mobility.

In (31), an expression is given for the mobility of a spherical particle with low but nonuniform zeta potential. The mobility in general depends on the orientation of the particle's quadrupole tensor  $\mathbf{Q}$  relative to the applied electric field. When averaged over orientations, the mean mobility depends only on the surface-averaged zeta potential  $\bar{\zeta}$ . The fluctuations in mobility due to orientational averaging of the one-particle mobility depend on the ratio of the quadrupole moment  $\sqrt{\mathbf{Q}:\mathbf{Q}}$  to  $\bar{\zeta}a^2$ . Assuming a value for this ratio of 1, which appears to be about the largest reasonable value, and averaging the quadrupole term over orientations (32), we

get relative rms fluctuations in velocity ranging from 3 to 16% as  $\kappa a$  varies from 1 to 10. More typical values of the quadrupole moment would give smaller values than this.

In summary, the contribution of particle interactions to velocity fluctuations appears to be comparable to that due to contributions from nonuniform potentials or a distribution of zeta potentials, but larger than that due to a distribution of particle size.

It has been assumed in this whole work that the suspension is actually a homogeneous liquid phase. It is possible in low-salt colloidal systems to produce gel-like and crystalline phases at very low volume fractions (around 1%). This illustrates the difference between the ‘‘hydrodynamic’’ volume fraction, which is what the term ‘‘volume fraction’’ means in this paper, and the ‘‘thermodynamic’’ volume fraction, i.e., the volume fraction at which liquid-like or solid-like ordering sets in. For such a system, if still fluid but with  $g(R)$  exhibiting liquid-like structure, presumably one should use the best estimate available for  $g(R)$  in the expressions for the suspension mobility and mean velocity fluctuations rather than the low (thermodynamic) density expression in Eq. [21]. For systems in a gel-like or crystalline state, the experiments envisaged in this analysis are not feasible, at least not with a static field.

Previous treatments of particle concentration effects for thick double layers have relied on cell model treatments, for low zeta potentials (33) or for higher zeta potentials but nonoverlapping double layers (34). The studies have shown quite significant effects especially at low porosities (high volume fractions) and low values of  $\kappa a$ . Several points need to be kept in mind when comparing our results with such cell model calculations.

The first is that the two techniques are aimed at complementary ranges of  $\phi$ . Our calculation is limited to low volume fractions since it considers only pair interactions. The cell model would be expected to be most valid at high volume fractions although it can be solved for any value of  $\phi$ . Comparing with Fig. 3 of (33) for  $\phi = 0.1$  and  $\kappa a \geq 1$ , we see reductions in electrophoretic mobility similar in magnitude to our results. However, this is somewhat misleading for reasons discussed below.

The second point is that the largest effects in (33) occur for  $\kappa a < 1$ . We have not considered such values in our work because such systems are rarely encountered. If the particles are small, the dispersions are barely stable and if the electrolyte concentration is very low, one may see the gel or crystal phases mentioned above.

Finally, the cell models do not appear to include the constraints that are necessary to renormalize the suspension mobility. There is no backflow and so no leading term of  $3/2\phi$  for thin double layers (see (34) Eq. [42]). In addition, the particle distribution is taken to be uniform and so it misses the effect of double-layer repulsion through the pair distribution function. These two effects act in opposite direc-

tions, which perhaps explains the rough agreement between the two approaches.

The main conclusion of this work, then, is that particle interaction effects can become significant for electrophoresis of systems with  $\kappa a$  around 1, with the magnitude of the effect dependent on the size of the particles. We would expect the results here, which are for low potentials, to be the upper bounds on the effect since higher zeta potentials are associated with somewhat thinner double layers and so lead to less particle interaction, in much the same way as the Deryaguin approximation for double-layer forces improves with surface potential (12).

One of the main systems relevant to these calculations are electrophoretic measurements of protein mobility (35). Experimental results for the concentration dependence of the mobility of proteins are available but are not discussed in terms of the effects calculated here (36). Instead they are interpreted in terms of changes in the ionic strength and hence  $\kappa$ , which we have not considered here. We hope to take up these points in the future.

### ACKNOWLEDGMENTS

The support of the Australian Research Council has made this work possible. S.L.C. and D.Y.C. also thank Professor John Anderson for a stimulating course on electrokinetics during his stay in Melbourne and Jonathon Ennis for sharing his insights and reflection results during this study.

### REFERENCES

- Hunter, R. J., "Zeta Potential in Colloid Science." Academic Press, New York, 1981.
- Dunstan, D. E., and White, L. R., *J. Colloid Interface Sci.* **152**, 297 (1992).
- Reed, L. D., and Morrison, F. A., *J. Colloid Interface Sci.* **54**, 117 (1976).
- Chen, S. B., and Keh, H. J., *AIChE J.* **34**, 1075 (1988).
- Keh, H. J., and Chen, S. B., *J. Colloid Interface Sci.* **130**, 542 (1989).
- Keh, H. J., and Chen, S. B., *J. Colloid Interface Sci.* **130**, 556 (1989).
- Keh, H. J., and Yang, F. R., *J. Colloid Interface Sci.* **145**, 362 (1991).
- Anderson, J. L., *Ann. Rev. Fluid Mech.* **21**, 61 (1989).
- Keh, H. J., and Chen, J. B., *J. Colloid Interface Sci.* **158**, 199 (1993).
- Kang, S., and Sangani, A., *J. Colloid Interface Sci.* **165**, 195 (1994).
- O'Brien, R. W., and White, L. R., *J. Chem. Soc. Faraday Trans. 2* **74**, 1607 (1978).
- Carnie, S. L., Chan, D. Y. C., and Stankovich, J., *J. Colloid Interface Sci.* **165**, 116 (1994).
- Teubner, M., *J. Chem. Phys.* **76**, 11 (1982).
- Ennis, J., and Anderson, J. L., *J. Colloid Interface Sci.* **185**, 497 (1997).
- Happel, J., and Brenner, H., "Low Reynolds Number Hydrodynamics." Noordhoff, Leyden, 1973.
- Kim, S., and Karrila, S. J., "Microhydrodynamics. Principles and Selected Applications." Butterworth-Heinemann, Boston, 1991.
- Davis, M. H., *J. Chem. Eng. Sci.* **24**, 1769 (1969).
- Stimson, M., and Jeffery, G. B., *Proc. R. Soc. London, A* **111**, 110 (1926).
- Spielman, L. A., *J. Colloid Interface Sci.* **33**, 562 (1970).
- Glendinning, A. B., and Russell, W. B., *J. Colloid Interface Sci.* **93**, 95 (1983).
- Kim, S., and Zukowski, C. F., *J. Colloid Interface Sci.* **139**, 198 (1990).
- Carnie, S. L., and Chan, D. Y. C., *J. Colloid Interface Sci.* **161**, 260 (1993).
- Carnie, S. L., Chan, D. Y. C., and Gunning, J., *Langmuir* **10**, 2993 (1994).
- Brady, J. F., and Durlofsky, L., *J. Fluid Mech.* **180**, 21 (1987).
- Ennis, J., and White, L. R., *J. Colloid Interface Sci.* **185**, 157 (1997); Erratum, in press.
- Batchelor, G. K., *J. Fluid Mech.* **52**, 245 (1972).
- Acrivos, A., Jeffrey, D. J., and Saville, D. A., *J. Fluid Mech.* **212**, 95 (1990).
- Zukoski, C. F., and Saville, D. A., *J. Colloid Interface Sci.* **115**, 422 (1987).
- Bell, G. M., Levine, S., and McCartney, L. N., *J. Colloid Interface Sci.* **33**, 335 (1970).
- Sader, J. E., Carnie, S. L., and Chan, D. Y. C., *J. Colloid Interface Sci.* **171**, 46 (1995).
- Yoon, B. J., *J. Colloid Interface Sci.* **142**, 575 (1991).
- Gray, C. G., and Gubbins, K. E., "Theory of Molecular Fluids. Volume 1: Fundamentals," p. 487. Clarendon, Oxford, 1984.
- Levine, S., and Neale, G. H., *J. Colloid Interface Sci.* **47**, 520 (1974).
- Kozak, M. W., and Davis, E. J., *J. Colloid Interface Sci.* **129**, 167 (1989).
- Douglas, N. G., Humffray, A. A., Pratt, H. R. C., and Stevens, G. W., *Chem. Eng. Sci.* **50**, 743 (1995).
- Mosher, R. A., Gebauer, P., Caslavská, J., and Thormann, W., *Anal. Chem.* **64**, 2991 (1992).